Fuel 284 (2021) 119285

Contents lists available at ScienceDirect

Fuel

journal homepage: www.elsevier.com/locate/fuel

Full Length Article

Effect of the support properties in dehydrogenation of biphenyl-based eutectic mixture as liquid organic hydrogen carrier (LOHC) over Pt/Al_2O_3 catalysts

Yeonsu Kwak [a], Seongeun Moon [a], Chang-il Ahn [a], Ah-Reum Kim [a], Yongha Park [a], Yongmin Kim [a], Hyuntae Sohn [a], Hyangsoo Jeong [a,d], Suk Woo Nam [a,b], Chang Won Yoon [a,c,d,*], Young Suk Jo [a,*]

[a] Center for Hydrogen and Fuel Cell Research, Korea Institute of Science and Technology (KIST), 5 Hwarang-ro 14-gil, Seongbuk-gu, Seoul 02792, Republic of Korea
[b] Green School, Korea University, Anam-ro 145, Seongbuk-gu, Seoul 02841, Republic of Korea
[c] KHU-KIST Department of Converging Science and Technology, Kyung Hee University, 26 Kyungheedae-ro, Dongdaemun-gu, Seoul 02447, Republic of Korea
[d] Division of Energy and Environment Technology, KIST School, Korea University of Science and Technology, Seoul 02792, Republic of Korea

ARTICLE INFO

Keywords:
Biphenyl
Liquid organic hydrogen carrier (LOHC)
Dehydrogenation
Hydrogen Production
Pt/Al_2O_3 catalysts
Alumina pellet

ABSTRACT

Biphenyl-based eutectic mixture (BPDM, 35 wt% Biphenyl, and 65 wt% Diphenylmethane) has gained attraction as a strong candidate for liquid organic hydrogen carriers (LOHC) particularly due to the high hydrogen capacity (6.9 wt%). To take full advantage of its capacity, facile and high-extent dehydrogenation with reversibility is the key, where the appropriate selection of supports in heterogeneous catalysts plays a crucial role. Herein, the effect of the properties of commercial Al_2O_3 pellets in the dehydrogenation reaction of a hydrogenated biphenyl-based mixture (H12-BPDM) over Pt/Al_2O_3 catalysts is investigated. H_2 production rate, 10 h performance tests, and product composition from the dehydrogenation of H12-BPDM are evaluated with the in-house catalytic screening tests using continuous fixed-bed reactors. Catalyst characterization and product analysis suggest that pore size distributions and corresponding surface properties of Al_2O_3 supports can lead to different dehydrogenation reaction characteristics of H12-BPDM. This study provides a rationale for the proper support selection for efficient utilization of BPDM as a LOHC.

1. Introduction

Hydrogen has been the center of attention for the clean and sustainable energy sources as it retains high energy density and produces low carbon emissions in the energy conversion processes via fuel cells, internal combustion engines, or turbines. [1,2] However, the low volumetric energy density of hydrogen has been the primary issue to be solved, where storing hydrogen in high pressure or cryogenic temperature still leaves a question in the efficiency, logistics, and safety. [3] Liquid organic hydrogen carriers (LOHCs), which store hydrogen in a variety of liquid chemicals in a stable manner under the ambient condition via catalytic hydrogenation/dehydrogenation, have been suggested as promising energy carriers to address the issues mentioned above. [4–6] Particularly, LOHCs can have larger gravimetric and volumetric energy density than compressed gas H_2. Energy density, economic feasibility, and practical applicability of numerous LOHCs including various cycloalkanes, N-heterocyclic hydrocarbons have been investigated. In the same context, the hydrogenation and dehydrogenation characteristics of LOHCs over various heterogeneous catalysts have also been thoroughly studied. [7–10]

Among the homocyclic cycloalkanes, Methylcyclohexane [11–20] (MCH, 6.16 wt% of H_2) and Perhydro-dibenzyltoluene [21–29] (H18-DBT, hydrogenated form of dibenzyltoluene, 6.24 wt% of H_2) have been highlighted since those are readily available in the industry and compatible with the existing fossil fuel-based storage and transport infrastructure. Notably, in the SPERA hydrogen project of Chiyoda Corporation, the H_2 storage and transport chain utilizing MCH/toluene as LOHC has been demonstrated by the consecutive cycles of hydrogenation and dehydrogenation over modified Pt/Al_2O_3 catalysts; the continuous dehydrogenation tests were conducted for 10,000 h in a pilot

* Corresponding authors at: Center for Hydrogen and Fuel Cell Research, Korea Institute of Science and Technology (KIST), 5 Hwarang-ro 14-gil, Seongbuk-gu, Seoul 02792, Republic of Korea.
E-mail addresses: cwyoon@kist.re.kr (C.W. Yoon), yjo@kist.re.kr (Y.S. Jo).

https://doi.org/10.1016/j.fuel.2020.119285
Received 3 July 2020; Received in revised form 15 September 2020; Accepted 17 September 2020
Available online 9 October 2020

scale. [30,31] Hydrogenious technologies designed and commercialized the H_2 production plant so-called the ReleaseUNIT using H18-DBT as LOHC to release H_2 in a medium-scale and large-scale [25], where Pt/Al_2O_3 catalysts also appear to be mainly utilized in the dehydrogenation process. [26,27] Bicyclohexyl (Hydrogenated form of biphenyl, 7.27 wt % of H_2) has gained attention as it shows not only the extremely high H_2 storage density in a weight basis but also the low enthalpy of dehydrogenation [32–35], but its practical technical application has been relatively limited mainly due to its low feasibility resulted from the high melting point (69.2 °C). Dicyclohexylmethane (Hydrogenated form of diphenylmethane, 6.71 wt% of H_2) captured the attention not only due to its H_2 capacity but also its availability as a model compound of more complex LOHCs such as DBT. [36–38] Recently, biphenyl-based eutectic mixture (BPDM) comprised of 35 wt% of Biphenyl and 65 wt% of Diphenylmethane has been suggested as a strong alternative as it can store up to 6.9 wt% of hydrogen where it remains liquid stably under the STP condition. [39–41] The major characteristics of common LOHCs and H12-BPDM are compared in Table S1.

To exploit its high hydrogen capacity in commercial applications, the rapid and energy-efficient catalytic dehydrogenation with full reversibility of LOHC would be particularly essential. The selection of proper heterogeneous catalysts for the dehydrogenation process would play a pivotal role. Al_2O_3, which has been widely recognized as a metal oxide support for various catalytic applications [17,42,43], has long been studied and adopted for MCH dehydrogenation not only for the fast kinetics, but also for the high activity, selectivity, and stability. Usman tested various Pt/Al_2O_3 catalysts with different alumina phases [11] and has studied the kinetics of alumina-based platinum catalysts over the MCH dehydrogenation. [12] Sugiura et al. and Yang et al. investigated Pt/TiO_2-modified Al_2O_3 catalyst to shift Pt binding energy and control the surface acidity, which improved catalytic performance. [13,14] Auer et al. boosted the H18-DBT dehydrogenation activity by adding sulfur on Pt/Al_2O_3 catalysts by blocking low coordinated defect sites and evaluated various alumina effects. [28] Meanwhile, in addition to the support engineering, the active sites modification by Pt-based alloy [44] has recently emerged as a promising strategy for MCH dehydrogenation. [15,16] Interpretation of MCH dehydrogenation mechanism [18,19] and feasibility analysis of new support materials [20] using density functional theory (DFT) have also been investigated.

Regarding biphenyl-based LOHCs, Kalenchuk et al. investigated the dehydrogenation characteristics of polycyclic naphthenic compounds including bicyclohexyl over the carbon-supported platinum catalysts [34] while proposing a biphenyl/bicyclohexyl couple as the best candidate by considering both the kinetic parameters and steric isomer effect. [35] However, to the best of our knowledge, hydrogen production and the dehydrogenation reaction characteristics of biphenyl-based LOHC over Pt/Al_2O_3 catalysts have not yet been studied in detail. In this study, we aimed to study the effect of commercially available 6 different pellet-type Al_2O_3 supports in the dehydrogenation of the hydrogenated biphenyl-based eutectic mixture (H12-BPDM) over Pt/Al_2O_3 catalysts. We synthesized 0.5 wt% monometallic Pt on commercial Al_2O_3 supports with a variety of pore size distribution and corresponding surface area. Then, catalytic activities were compared using in-house performance screening tests at different temperatures, LHSV, and H_2 co-feeding rates. Finally, the reaction characteristics of H12-BPDM on Pt/Al_2O_3 catalysts were correlated to the catalyst characterization involving Pt nanoparticle morphology, metal-support interaction, and support acidity.

2. Experimental

2.1. Materials

High-purity biphenyl and diphenylmethane were purchased from Sigma-Aldrich (US) and Tokyo Chemical Industry (Japan), respectively, and used without further purification. Hydrogen-lean biphenyl mixture (BPDM) was prepared by mixing 35 wt% of biphenyl and 65 wt% of diphenylmethane. The eutectic mixture was hydrogenated by the method published elsewhere. [39,40] 0.5 wt% Pt/Al_2O_3 model catalyst (denoted as Pt/A (0)) was purchased from Sigma-Aldrich. Al_2O_3 supports (denoted as A (1) – A (6), arranged in the order of manufacturer's serial number) were purchased from Alfa Aesar and used as-received, where the basic characteristics and information are given in Table S2. Hexachloroplatinic acid hexahydrate ($H_2PtCl_6 \cdot 6H_2O$, 37.5 wt% of Pt, Sigma Aldrich) was used as a Pt precursor in this study.

2.2. Catalyst preparation

Pt/Al_2O_3 catalysts were synthesized via wetness impregnation. In the procedure, 0.067 g of $H_2PtCl_6 \cdot 6H_2O$ (37.5 wt% of Pt) was dissolved in deionized water (DIW) at 20 °C. Al_2O_3 supports were dried at 110 °C for 72 h, and then the Pt precursor solution in DIW was added to 5 g of each dried Al_2O_3 support. Then, the mixtures were stirred and dried in a vacuum oven at 110 °C overnight to obtain a dried and well-distributed precursor. Calcination was carried out in a muffle furnace at 450 °C for 3 h with a ramp of 10 °C/min. After cooling to ambient temperature, 0.5 wt% Pt (nominal amount)/Al_2O_3 catalysts (denoted as Pt/A (1) – Pt/A (6)) were prepared, where the key features are provided in Table 1. Catalysts were in-situ reduced using a 20 mL/min of H_2 at 400 °C for 30 min before the catalytic performance tests or long-term tests.

2.3. Catalyst characterization

The BET surface area and BJF pore size distribution of the samples were measured at 77 K by N_2 physisorption (ASAP 2000, Micromeritics). Before the measurement, samples were dried at 250 °C in a vacuum (<30 mmHg) overnight. The exact amount of bulk Pt content in the samples was measured using inductively coupled plasma-optical emission spectroscopy (ICP-OES, OPTIMA 5300DV, PerkinElmer). Before the analysis, samples were pre-treated with the acid digestion sample preparation methods using HCl, HF, and HNO_3. The amount of Pt was detected at a wavelength of 265.945 nm with 1.3 kW of radio frequency power. The qualitative and semi-quantitative composition of the samples is shown in Table 2 using x-ray fluorescence spectroscopy (XRF, ZSX Primus II, Rigaku) at 50 kV and 30 mA for heavy elements (Ti – U), 40 kV and 75 mA for Ca and K, and 30 kV and 100 mA for light elements (Cl – B). The crystalline structure and particle size of the samples were analyzed by X-ray diffractometer (XRD, MiniFlex II, Rigaku) at 30 kV and 15 mA using Cu Kα wavelength ($\lambda = 0.154$ nm) using a continuous scanning mode from 10° to 70° with a scanning rate of 2°/min. The chemical states of Pt over the as-synthesized and used Pt/Al_2O_3 catalysts were analyzed by X-ray photoelectron spectroscopy (XPS, K-Alpha, Thermo Fisher Scientific) calibrated by C1s peak at 284.5 eV. Morphologies of Pt/Al_2O_3 catalysts and particle size distributions of Pt nanoparticles were analyzed using scanning electron microscopy-energy dispersive X-ray spectrometer (SEM: Inspect F50, FEI, EDS: Apollo X, EDAX Inc.) and transmission electron microscopy (TEM, TitanTM 80–300, FEI).

Temperature-programmed desorption (NH_3-TPD), temperature-programmed reduction (H_2-TPR), and pulse CO-Chemisorption (CO-Chemi) were conducted on the automated catalyst characterization system (AutoChem II 2920, Micromeritics) with thermal conductivity detector (TCD). To evaluate the acidity of samples, NH_3-TPD was conducted from 100 °C to 700 °C with a ramp of 10 °C/min after the pre-treatment using He at 600 °C for 1 h and the adsorption of NH_3 at 100 °C for 30 min. To investigate the reduction mechanism, H_2-TPR was conducted from 100 °C to 700 °C with a ramp of 10 °C/min using 25 mL/min of 10% (vol/vol) H_2 in Ar mixture after the pre-treatment using Ar at 200 °C for 1 h. CO-Chemi was conducted at 50 °C using a 1 mL injection of 20 mL/min of 10% (vol/vol) CO in He with an interval of 4 min after the pre-treatment of 20 mL/min of H_2 at 400 °C for 30 min and the purging of 20 mL/min of Ar at 400 °C for 30 min. The stoichiometric

Table 1
BET surface area, pore volume analysis and Pt loading of Pt/A (0) – (6).

Entry	Mfr. - Serial Number	S_{BET} (m^3/g)	V_{total} (cm^3/g)	Pt loading [a] (wt.%)	Dispersion [b] (%)	Pt <d_p> [b] (nm)	Pt <d_{avg}> [c] (nm)
Pt/Al_2O_3 (0)	Sigma Aldrich - 206016	105.8	0.23	0.47	49.3	1.92	1.86
Pt/Al_2O_3 (1)	Alfa Aesar - 43832	247.1	0.78	0.433	79.7	1.18	1.58
Pt/Al_2O_3 (2)	Alfa Aesar - 43855	222.3	0.60	0.447	78.0	1.21	1.60
Pt/Al_2O_3 (3)	Alfa Aesar - 43856	35.7	0.13	0.470	69.6	1.36	1.68
Pt/Al_2O_3 (4)	Alfa Aesar - 43857	116.7	0.49	0.464	76.0	1.24	1.65
Pt/Al_2O_3 (5)	Alfa Aesar - 43862	0.25	0.26	N/A*	–	–	–
Pt/Al_2O_3 (6)	Alfa Aesar - 44849	0.67	0.0002	N/A*	–	–	–

[a] Pt loading from ICP-OES. *immeasurable as insoluble in acid solution
[b] Metal dispersion, cubic crystallite size estimated from CO-chemisorption.
[c] Averaged particle size from HAADF-STEM images.

Table 2
XRF results of as-synthesized Pt/A (1) - (4).

(mass%)	Pt	Al	O	Si	Na	Mg	Cl
Pt/A (1)	1.29	49.9	48.1	0.04	–	–	0.63
Pt/A (2)	1.52	50.8	46.9	0.07	–	–	0.63
Pt/A (3)	1.02	31.5	46.5	15.9	0.44	0.28	0.13
Pt/A (4)	1.29	51.9	46.3	0.01	–	–	0.37

Table 3
Composition of organic liquid products from 10 h performance tests of Pt/A (0) – (4).

[Area%]	L0	L1	L2	L3	L4
Reactant BC	10.0%	11.7%	10.5%	5.4%	7.6%
Reactant DCM	25.4%	22.8%	23.4%	7.5%	16.8%
Intermediate CB	8.1%	7.2%	6.1%	5.3%	5.3%
Intermediate CMB	20.8%	21.0%	17.6%	16.6%	16.3%
Product BP	7.8%	11.5%	11.9%	27.4%	18.4%
Product DPM	27.7%	25.7%	30.2%	37.3%	35.1%
Cracked Product (Benzene, Toluene)	0.1%	0.0%	0.1%	0.1%	0.1%
Isomerized Product (Perhydro-fluorene)	0.2%	0.1%	0.1%	0.4%	0.6%

(BC, Bicyclohexyl; DCM, Dicyclohexylmethane; CB, Cyclohexylbenzene; CMB; Cyclohexylbenzylmethane; BP, Biphenyl; DPM, Diphenylmethane)

ratio of which CO/Pt (mol/mol) = 1 and the spherical particles of Pt are assumed to calculate the dispersion of samples.

2.4. In-house catalyst screening tests

A high-throughput catalytic screening system capable of conducting multiple tests on continuous packed bed reactors was constructed and used for the dehydrogenation of H12-BPDM. A process flow diagram (PFD) and the configuration of each continuous reactor are shown in Fig. 1. H12-BPDM was supplied to a reactor by a high-pressure liquid chromatography pump (Series II Legacy HPLC pump, Teledyne SSI). The reaction temperature of the packed bed was controlled by the electrical furnace, where the controlling temperatures are measured by K-type thermocouples in the middle of the catalytic bed. LOHC feeds are pre-heated via inert SiC beads and glass fibers (Pyrogel XT-E, Aspen Aerogels, US).

For dehydrogenation performance tests in various operation conditions, 0.5 wt% Pt /Al_2O_3 pellet catalysts (Pt/A (0) – Pt/A (6), 2 g) were packed in a tubular reactor (O.D. 1/2″, stainless steel). In regards to the operation conditions, atmospheric pressure (=1 bar(a)) was remained in the entire procedure, while dehydrogenation temperature was varied at 280 – 340 °C and liquid hourly space velocity (LHSV) was varied at 0.6 – 1.7 mL/g_{cat}/h. Hydrogen was co-fed to the dehydrogenation reactor since hydrogen partial pressure has been known for its role to protect catalyst deactivation. [45] The mixing ratio of H_2 to LOHC was varied from 0 to 3 on a molar basis. For GC–MS composition verification tests, Pt/Al_2O_3 catalysts (Pt/A (0) – Pt/A (4), 2 mL) were packed in the same manner, and the test was carried out for 10 h at 320 °C, pressure = 1 bar (a), LHSV = 1 mL/mL_{cat}/h, and H_2/LOHC = 0.84 mol/mol. Product mixtures including dehydrogenated and unreacted H12-BPDM were cooled and separated at a vapor–liquid separator in atmospheric temperature. Zeolite (molecular sieve 13X, Sigma-Aldrich) was activated at 300 °C for 15 h and used as an adsorbent material to remove remaining organics in the produced hydrogen after the vapor–liquid separator.

2.5. Product analysis

Flowrates of the produced hydrogen were measured using an H_2 mass flow meter (H_2-MFM, F-201CL, Bronkhorst) and converted to the catalytic activity of H12-BPDM dehydrogenation by the eq. (1), which is equivalent to the catalytic conversion factor. Composition of liquid organic products was analyzed using the data obtained from the gas chromatography-mass spectrometry (GC–MS, GC: 6890 N GC, Agilent Technologies, MS: Pegasus IV, LECO) using DB-5MS column (30 m × 0.25 mm × 0.25 um) with an elevated oven temperature from 40 °C to 280 °C with a ramp of 10 °C/min.

$$\text{Degree of Dehydrogenation: DoDH } (\%) = \frac{\text{Released } H_2 \text{ (mL/min)}}{\text{Theoretical } H_2 \text{ (mL/min)}} \cdot 100 \quad (1)$$

3. Results and discussion

3.1. Characterization of the as-synthesized Pt/Al_2O_3 catalysts

In Fig. 2(a) and Table 1, N2 physisorption data shows that the BET surface area are in the order of: Pt/A (1) > Pt/A (2) > Pt/A (4) > Pt/A (0) > Pt/A (3) and the mode of pore size is in the reverse order. In the case of Pt/A (5) and Pt/A (6), N_2 physisorption at 77 K could not produce isotherms and relevant data due to the low surface area. In Fig. 2 (b), XRD data confirms that Pt/A (0), Pt/A (1), and Pt/A (2) contain the distinctive peaks of gamma-alumina (γ-Al_2O_3), while Pt/A (5) and Pt/A (6) exhibit alpha-alumina (α-Al_2O_3) peaks, and Pt/A (4) is mainly theta-alumina (θ-Al_2O_3). Pt/A (3) is partly composed of θ-Al_2O_3 peaks, but rather a peak related to SiO_2 was observed, which is compatible with the XRF result in Table 2.

Morphologies of Pt/Al_2O_3 catalysts and particle size distributions of Pt nanoparticles are shown in Fig. 3(a) -Fig. 3(e). In SEM analysis, the pore characteristics of each Al_2O_3 were observable, where Pt/A (3) has less pore and wrinkled structure, whereas Pt/A (0), (1), (2), and (4) showed lots of sub-micrometer grains on the surface. (Fig. 3(a1) – Fig. 3 (e1)) However, Pt nanoparticles were not detectable via EDX analysis due to its small sizes and low content. To further examine the distribution of Pt particles, TEM and HAADF-STEM analyses were conducted, which are shown from Fig. 3(a2) to Fig. 3(e2) and Fig. 3(a3) to Fig. 3 (e3), respectively. Based on the STEM images, the size and distribution

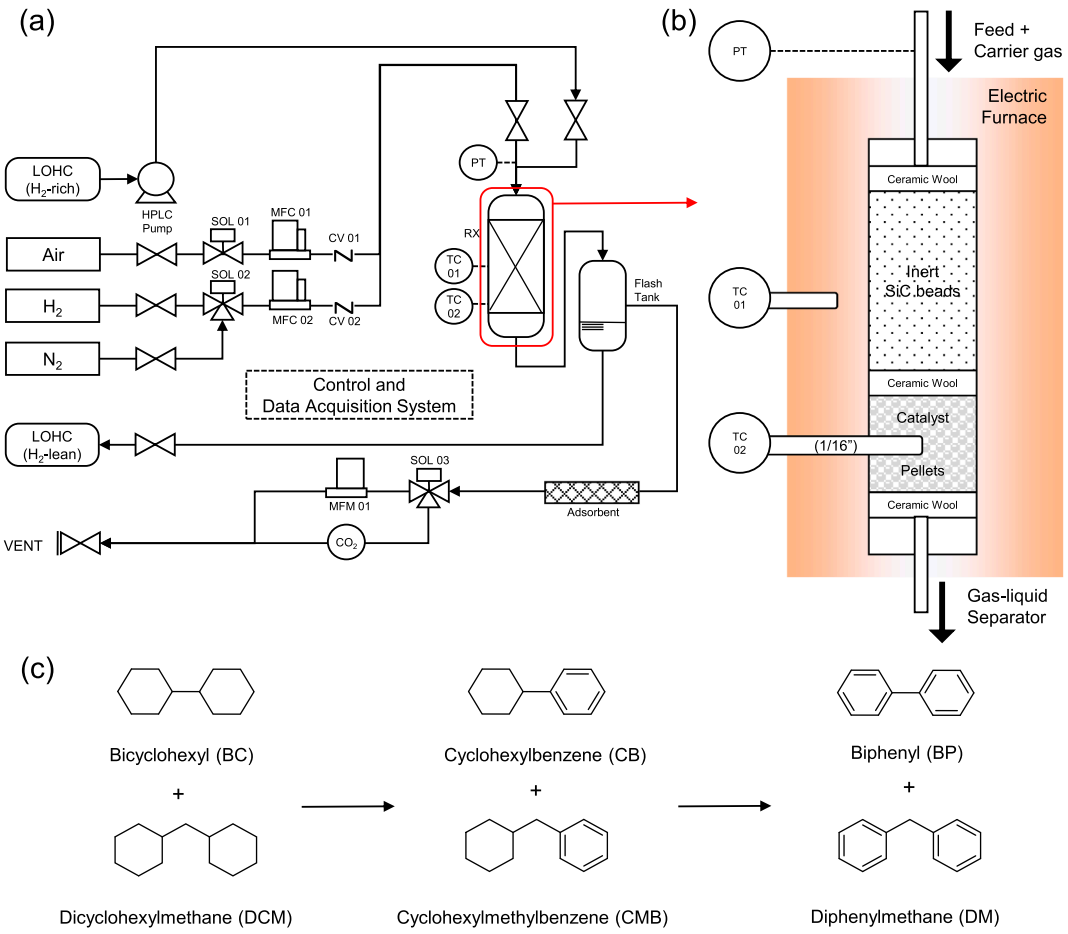

Fig. 1. (a) Schematic diagram of the high-throughput catalytic screening system for LOHC dehydrogenation. (b) Configuration of each catalytic bed. (c) Schematic of dehydrogenation reaction of H12-BPDM.

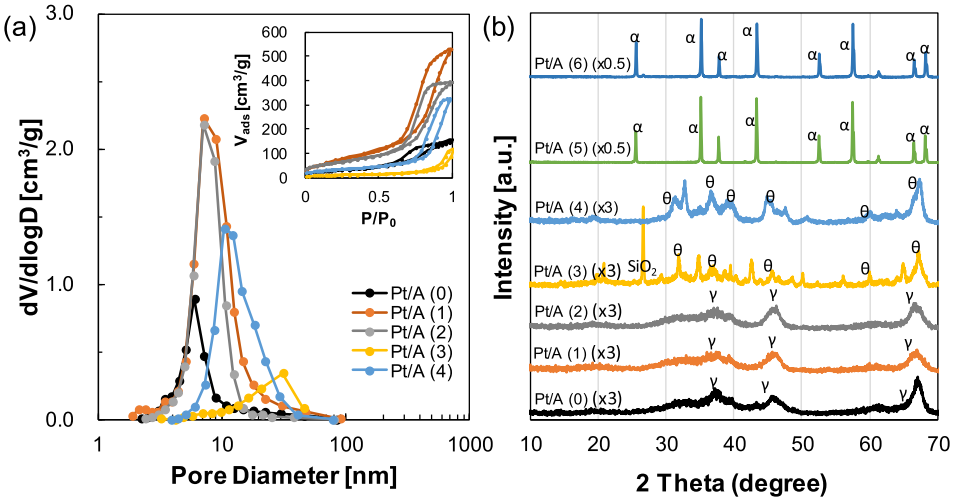

Fig. 2. Characteristics of Pt/Al_2O_3 catalysts: (a) Pore size distribution and N_2 adsorption/desorption isotherm of Pt/A (0) – (4). (b) XRD patterns for Pt/A (0) – (6). (For interpretation of the references to color in this figure legend, the reader is referred to the web version of this article.)

of Pt nanoparticles were obtained. Conducting image analysis over 200 – 250 particles from Pt/A (0) to Pt/A (4), the average size of Pt particles was in the order of Pt/A(0) > Pt/A (3) > Pt/A (4) > Pt/A (2) > Pt/A (1), which is compatible with the tendency of Pt cubic crystalline size obtained from CO-chemisorption (see Table 1). However, there was a difference in the particle size distribution, where Pt/A (0) and Pt/A (3) showed relatively broad and narrow peak, respectively, while Pt/A (1), (2), and (4) displayed similar patterns in terms of width and shape, close to normal Gaussian curves. It is due to the egg-shell type coating and the fact that the fabrication process of the commercial Pt/A (0) could entail the calcination in a certain temperature that can lead Pt precursors to have coalesced. The eccentricity of Pt/A (3) can be also explained by the

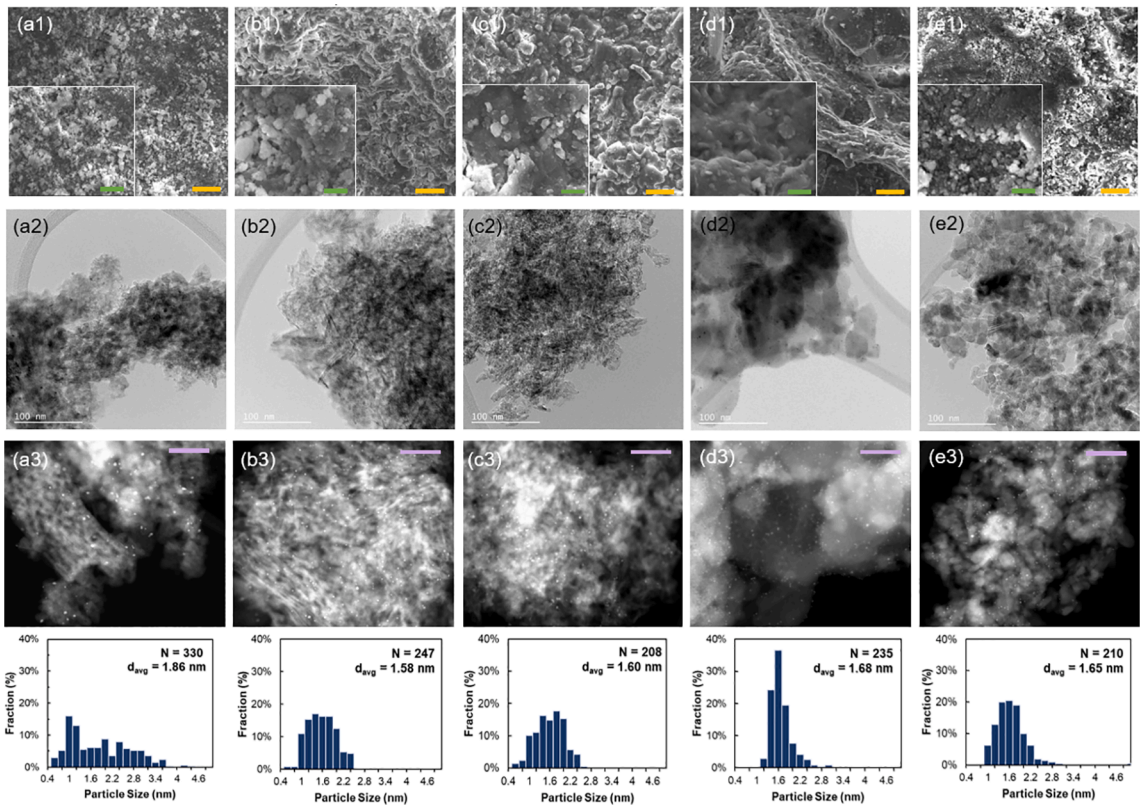

Fig. 3. (a1 – e1) SEM images of Pt/A (0) – (4) (Scale Bar: Light Green = 2 μm, Yellow = 10 μm) (a2 – e2) TEM images of Pt/A (0) – (4) (Scale Bar: White = 100 nm) (a3 – e3) HAADF-STEM images and particle size distributions of Pt/A (0) – (4) (Scale Bar: Violet = 50 nm). (For interpretation of the references to color in this figure legend, the reader is referred to the web version of this article.)

compositional discrepancy, as the XRF result in Table 2 showed that Pt/A (3) contains SiO_2 along with Al_2O_3, and a trace amount of Na and Mg which can play a role of additives for Pt. [46]

3.2. Catalytic dehydrogenation of H12-BPDM

In Fig. 4, the effect of temperature, LHSV (catalyst weight basis, from Fig. 4(a) to Fig. 4(c), catalyst volume basis in Fig. 4(d)), and H_2/LOHC ratio (mol/mol) over the degree of H12-BPDM dehydrogenation (DoDH, i.e., catalytic conversion) were evaluated respectively while controlling the other parameters to be constant. In the tests under the same LHSV, in Fig. 4(a), Fig. 4(c), Fig. 4(d) and Fig. 4(f), the y-axis number range (0 – 100) can be also interchanged with H_2 productivity (P_{H2}, $mmol_{H2}/g_{met}$/min). Throughout the tests in catalyst weight basis, Pt/A (1) showed the superior activity while Pt/A (3), Pt/A (2), Pt/A (4), Pt/A (0), Pt/A (5), Pt/A (6) sequentially followed. The consecutive activities of Pt/A (1), Pt/A (2), Pt/A (4), Pt/A (5), and Pt/A (6) seem to be primarily attributed to the dispersion of Pt, which is related to the number of approachable Pt nanoparticles on the catalyst, which is presented in Table 1. The high dispersion can be related to the porous structure which leads to strong metal-support interaction by stabilizing small metal clusters on the surface. [47] It is also observed that surface acidity can be positively correlated with the surface area as a complexity factor of the support structure. (Fig. 5(a)) Pt/A (5) and Pt/A (6), which has no mesoporous structure developed in the support (see Table 1) with α-Al_2O_3 structure, showed no prominent activities compared to the Pt/A (0) – (4) in the same screening tests, thus the used catalysts and products were not analyzed further. However, it should be mentioned that the commercial pellet comprising α-Al_2O_3 with a well-structured mesoporous structure is of interest for future studies. Meanwhile, Pt/A (3) showed decent activity despite its very low surface area, and the activity is even more than one of either Pt/A (2) or Pt/A (4), which is possibly due to the synergistic effect between SiO_2 and Al_2O_3 [48,49] and impurity metals (K, Ca) acting as promoters [50,51] which is originally contained in the A (3). For testing durability, we conducted a 10 h performance test. (Fig. 4(d)) Here, we found that Pt/A (1) remained 91.8% of DoDH after 10 h, which is equivalent to 92.6 $mmol_{H2}/g_{cat}$/h and Pt/A (3) remained 90.0% of DoDH, which is tantamount to 90.74 $mmol_{H2}/g_{cat}$/h.

We conducted NH_3-TPD and H_2-TPR experiments to understand surface characteristics as well as to investigate the eccentric performance of Pt/A (3), as shown in Fig. 5, Table 4, and Table 5. It has been reported that the first peak around 200 – 300 °C is due to the reduction of the bulk PtO_x weakly interacting with Al_2O_3 or the reduction of chloride-containing species [52], while the second peak around 300 – 400 °C refers to the PtO_x portions that strongly interact with the support. While Pt/A (1), (2), and (4) showed H_2-TPR trends comparable with previously reported data for Al_2O_3 [53], it is revealed that Pt/A (3) only uptakes a lot of hydrogen after 400 °C. The enhanced performance of Pt/A (3) can be derived from the Pt or additive metals that strongly interacts with the support. H/Pt ratio (mol/mol) was calculated based on the hydrogen uptake amount and it can be observed that commercial Pt/A (0) (H/Pt < 1) is in a reduced form and most of the Pt remains its metallic state in the atmospheric condition. (Fig. 5(b)) Pt/A (1), (2), and (4) showed H/Pt ≅ 2, which refers that as-synthesized catalysts are prepared in Pt^{2+} form. Pt/A (3) showed the highest H/Pt ratio of 4, where it is expected as a role of various oxides from the impurity metals, rather than Pt^{4+} whose peak can occur in 95 – 105 °C. [54]

The performance of the catalyst on a volume basis can be an important criterion to select a proper pellet catalyst, considering applications with limited system volume. In Fig. 4(e), the effect of LHSV (mL/mL_{cat}/h, catalyst volume basis) on the catalytic activity of H12-BPDM dehydrogenation at 300 °C was compared. Notably, Pt/A (0) – (4) catalysts showed comparable performance in a catalyst volume basis. Thus, we tried to investigate the difference in each performance in terms

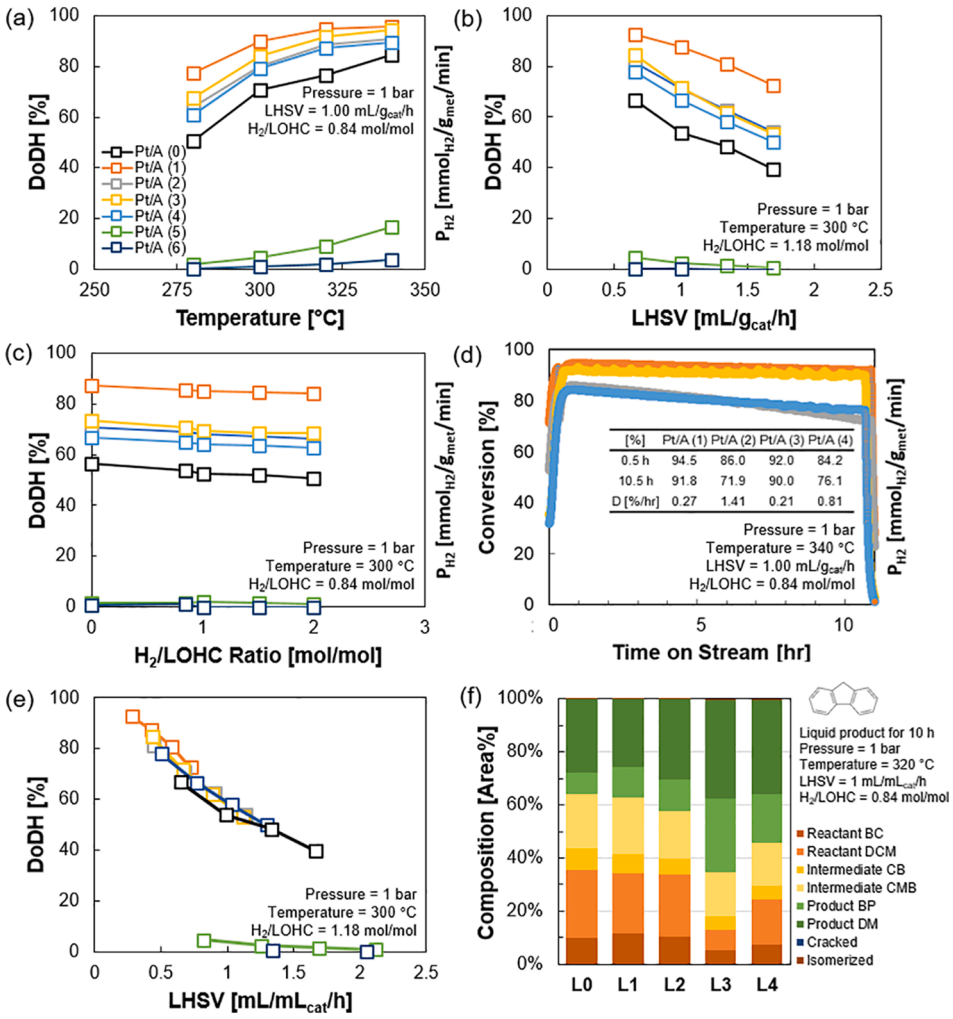

Fig. 4. In-house catalytic screening test results of BPDM dehydrogenation over Pt/A (0) – (6): (a) Temperature, (b) LHSV (0.7 – 1.7 mL/g_{cat}/h), (c) H_2/LOHC ratio, (d) 10 h performance tests, (e) LHSV (0.3 – 2 mL/mL_{cat}/h). (f) Organic liquid composition by GC–MS. (For the interpretation of the references to color in this figure legend, the reader is referred to the web version of this article.)

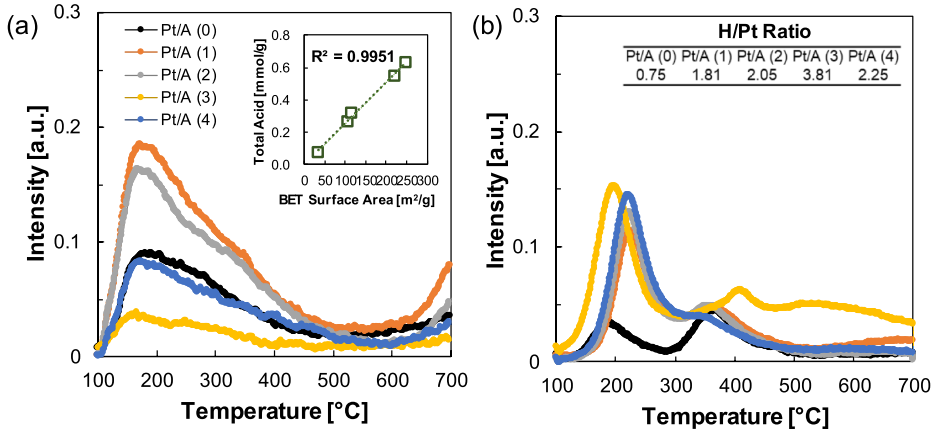

Fig. 5. (a) NH_3-TPD result of Pt/A (0) – (4) and the relationship between surface complexity and total acid (inset), (b) H_2-TPR results of Pt/A (0) – (4) and H/Pt ratio of each catalyst (inset).

of organic liquid product (H_2-lean BPDM) composition using GC/MS at a higher temperature at 320 °C. In Fig. 4(f), the GC/MS area-based compositions of organic liquid products obtained from 10 h performance tests at LHSV = 1 mL/mL_{cat}/h is illustrated to estimate the degree of dehydrogenation as well as to verify the presence of byproducts via cracking and isomerization, also given in Table 3. The organic liquid product from the Pt/Al_2O_3 (0) – (4) catalyst is denoted as L0 – L4. Note that LHSV = 1 mL/mL_{cat}/h is relatively high space velocity compared to LHSV = 1 mL/g_{cat}/h due to the low packing density of the Pt/A pellets (<1 g/mL). We first observed that the degree of dehydrogenation

Table 4
Acid properties Pt/A (0) – (4) from the NH_3-TPD experiment.

Samples	T1 (°C)	Fraction 1[%]	T2 (°C)	Fraction 2[%]	T3 (°C)	Fraction 3[%]	Total Acid ($mmol_{NH3}/g_{cat}$)
Pt/A (0)	123.1	2%	179.9	79%	286.2	18%	0.266
Pt/A (1)	121.1	3%	177.9	86%	323.5	12%	0.634
Pt/A (2)	120.6	3%	176.1	86%	335.0	11%	0.550
Pt/A (3)	120.3	3%	159.4	39%	263.9	58%	0.078
Pt/A (4)	121.9	3%	179.1	82%	362.0	15%	0.319

Table 5
Reduction properties Pt/A (0) – (4) from the H_2-TPR experiment.

Samples	T1 (°C)	Fraction 1 [%]	T2 (°C)	Fraction 2 [%]	T3 (°C)	Fraction 3 [%]	Total H_2 consumed ($mmol_{H2}/g_{cat}$)
Pt/A (0)	188.1	39%	362.3	61%			0.019
Pt/A (1)	224.4	48%	353.2	52%			0.046
Pt/A (2)	222.1	50%	345.9	50%			0.053
Pt/A (3)	196.4	38%	410.4	37%	593.6	25%	0.098
Pt/A (4)	222.4	63%	317.9	37%			0.058

calculated from the organic liquid product in an order of Pt/A (3) > Pt/A (4) > Pt/A (2) > Pt/A (1) ≅ Pt/A (0), which is obviously different from the tendency in LHSV = 1 $mL/g_{cat}/h$. As Pt nanoparticle formation between Pt/A (1) - (2) and Pt/A (3) – (4) showed not much difference in average size and particle size distribution, we can interpret the tendency as the Pt content in the unit volume of each pellet simply leads to the difference in performance. No observable peaks were found in cracked products other than benzene and toluene, and the compositions of benzene and toluene in the organic liquid product are around 0.1%. It is revealed that the surface acidity of the Al_2O_3 (Fig. 5(a)) does not affect the number of cracked or isomerized products, as Pt/A (1) with the highest unit acid amount (0.634 $mmol_{NH3}/g_{cat}$, see Table 4) does not generate much benzene, toluene, or 9H-Fluorene, whereas a fraction of isomerized products was rather detected in Pt/A (3) and Pt/A (4), where the degree of dehydrogenation reaction is higher. Pt/A (3) and Pt/A (4) generated 0.4% and 0.6% of 9H-Fluorene, while γ-Al_2O_3 based Pt/A (0) – (2) gave rise to at around 0.1% of such byproduct. We observed the degree of cyclization, 9H-Flourene generation from diphenylmethane in Pt catalysts [29,55], which is proportional to DoDH regardless of the surface acidity. Similar This byproduct should be minimized as its high melting point (~116 °C) can lead to a clogging and transportation issue, while we expect that this can be mitigated with γ-Al_2O_3 based Pt catalysts.

3.3. Post-mortem analysis

Catalysts after catalyst performance tests were collected for post-catalysis analysis. (Fig. S1) As-synthesized catalysts revealed yellow colors as it contains around 0.1 – 0.6 mass% of Chlorine contents (see Table 2) as the H_2PtCl_6 $6H_2O$ precursor can be fully reduced into Pt in 500 °C, which is higher than the static-air calcination temperature in this study (450 °C). After catalysis, however, in-situ reduction in 400 °C performed before analysis might lead to the full evaporation of chlorine contents and leave Pt only, as its color and the previous study indicate. [56] N_2 physisorption over as-received supports, as-synthesized Pt/Al_2O_3 catalysts, and catalyst performance-tested Pt/Al_2O_3 was carried out to observe any difference in Al_2O_3 pores after the BPDM dehydrogenation (Fig. 6). It seemed that Pt impregnation, calcination, and long-

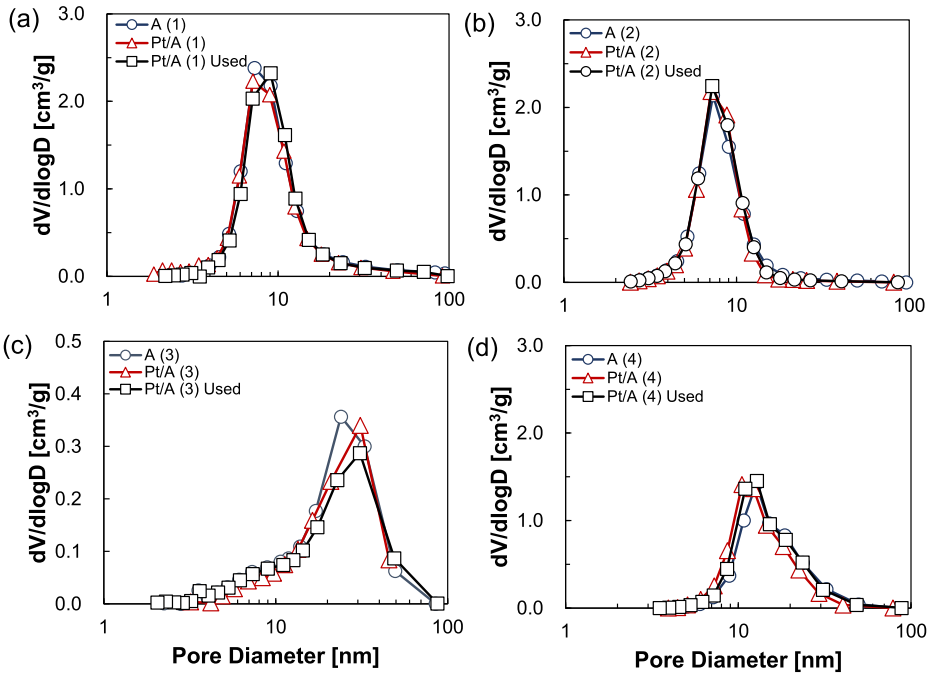

Fig. 6. Pore size distribution of as-received Al_2O_3, as-synthesized Pt/A, performance-tested Pt/A (1) - (4).

term dehydrogenation do not affect the quantity or the quality of Al_2O_3 pores.

XPS analysis was conducted over as-synthesized and tested Pt/A (1) - (4) to observe the oxidation state of Pt after the synthesis and after the reaction. Although a large number of previous reports related to Pt-based heterogeneous catalysts showed chemical states of Pt by using Pt 4f levels, we utilized $4d_{5/2}$ level data to avoid overlapping problems of Al 2p and Pt 4f energy levels [57] (Fig. S2). The binding energies of main core Pt 4d peaks for all fresh and used catalysts were in the order of Pt/A (3) > Pt/A (4) > Pt/A (2) > Pt/A (1). Although metallic Pt and PtO_x are presumed to coexist in Pt/Al_2O_3 catalysts, in XPS Pt^0 is primarily detected while apparent peaks of PtO (317.3 eV) and PtO_2 (318.6 eV) were not found. Generally, it is known that the small sizes of metal particles lead to binding energy shifts to higher energy levels. [58] Additionally, gamma-phase alumina is known to be able to interact more strongly with Pt nanoparticles than the alpha-phase alumina. However, it was difficult to find a significant correlation between Pt 4d level binding energies and Pt particle size or different phases of alumina possibly due to the similar Pt nanoparticle size (around 1–2 nm) along with the low contents (0.5 wt%) of Pt metal on the surface of catalysts, where 50 times of scan still gave rise to an interior signal-to-noise ratio. Since all the catalysts were used via the in-situ reduction process, the shift of Pt core peaks to lower binding energy (<314.6 eV) was observed in all cases. This also means that reduced metallic Pt phases in Pt/A (1) - (4) are well maintained during the dehydrogenation reaction and after the reaction.

4. Conclusion

We studied the effect of various commercial Al_2O_3 supports on the dehydrogenation of the hydrogenated biphenyl-based mixture (H12-BPDM) over 0.5 wt% Pt/Al_2O_3 (commercial pellet) catalysts synthesized from the wet impregnation method. In the activity tests, Pt/A (1) - (4) using the supports with a fairly large amount of surface area (>30 m^2/g) showed comparable performance, while Pt/A (5) and (6) using the supports with the immeasurably low surface area indicated weak activities. In a comparison of mass activity at the same LHSV of 1 $mL/g_{cat}/min$, Pt/A (1) with γ-Al_2O_3 showed the best performance primarily due to the high dispersion, where eccentric high performance was observed with Pt/A (3), which might be attributed to the additives and synergistic effect of SiO_2 and Al_2O_3. In 10 h durability tests in the LHSV of 1 $mL/g_{cat}/min$ at 340 °C, Pt/A (1) and Pt/A (3) maintained performance above 90% of DoDH, which is equivalent to ca. 90 $mmol_{H2}/g_{cat}/h$. In 10 h performance tests in the same LHSV of 1 $mL/mL_{cat}/min$ at 320 °C, Pt/A (3) showed the best activity but Pt/A (3) and (4) displayed an unignorable amount (up to 0.6%) of isomerized products that need to be mediated. A post-catalysis study showed that the metallic states and pore structures remained intact after the dehydrogenation of H12-BPDM over Pt/Al_2O_3 catalysts. This study would provide fundamentals to choose proper commercial pellet type supports for active, selective, and stable dehydrogenation, which can help the further development of modified or multicomponent Pt/Al_2O_3 catalysts or the technical application of BPDM dehydrogenation in large-scale H_2 production.

LOHCs are expected to be one of the efficient energy storage options allowing transport of renewable energy in a form of hydrogen; they can be used for both centralized and distributed hydrogen extraction systems. Also, LOHCs are potentially applicable to mobility solutions such as fuel cell trucks or trains. Therefore, to make LOHCs more practical and economically feasible, there would be next steps following such as the low-temperature dehydrogenation beyond the equilibrium limitation, the fabrication of an energy-efficient dehydrogenation reactor with much less energy consumption, the enhancement of Al_2O_3 through a synergistic approach using thermally conductive supports, and the low dosage of noble metals via direct deposition to considerably lower the catalyst price.

CRediT authorship contribution statement

Yeonsu Kwak: Conceptualization, Methodology, Investigation, Writing - original draft. **Seongeun Moon:** Investigation, Validation. **Chang-il Ahn:** Validation, Writing - review & editing. **Ah-Reum Kim:** Investigation. **Yongha Park:** Validation. **Yongmin Kim:** Resources. **Hyuntae Sohn:** Resources. **Hyangsoo Jeong:** Resources. **Suk Woo Nam:** Resources. **Chang Won Yoon:** Project administration, Funding acquisition. **Young Suk Jo:** Conceptualization, Supervision, Writing - review & editing.

Declaration of Competing Interest

The authors declare that they have no known competing financial interests or personal relationships that could have appeared to influence the work reported in this paper.

Acknowledgments

This work was supported financially by a National Research Foundation (NRF) grant funded by the Korean government (Ministry of Science, ICT & Future Planning) [grant number NRF-2019M3E6A1064611] and by the KIST institutional program of the Korea Institute of Science and Technology [grant number 2E30201, 2E30202].

Appendix A. Supplementary data

Supplementary data to this article can be found online at https://doi.org/10.1016/j.fuel.2020.119285.

References

[1] Abdin Z, Zafaranloo A, Rafiee A, Mérida W, Lipiński W, Khalilpour KR. Hydrogen as an energy vector. Renew Sustain Energy Rev 2020;120:109620. https://doi.org/10.1016/j.rser.2019.109620.
[2] White C, Steeper R, Lutz A. The hydrogen-fueled internal combustion engine: a technical review. Int J Hydrogen Energy 2006;31(10):1292–305. https://doi.org/10.1016/j.ijhydene.2005.12.001.
[3] Abe JO, Popoola API, Ajenifuja E, Popoola OM. Hydrogen energy, economy and storage: Review and recommendation. Int J Hydrogen Energy 2019;44(29):15072–86. https://doi.org/10.1016/j.ijhydene.2019.04.068.
[4] Modisha PM, Ouma CNM, Garidzirai R, Wasserscheid P, Bessarabov D. The Prospect of Hydrogen Storage Using Liquid Organic Hydrogen Carriers. Energy Fuels 2019;33(4):2778–96. https://doi.org/10.1021/acs.energyfuels.9b00296.
[5] Aakko-Saksa PT, Cook C, Kiviaho J, Repo T. Liquid organic hydrogen carriers for transportation and storing of renewable energy – Review and discussion. J Power Sources 2018;396:803–23. https://doi.org/10.1016/j.jpowsour.2018.04.011.
[6] Preuster P, Papp C, Wasserscheid P. Liquid Organic Hydrogen Carriers (LOHCs): Toward a Hydrogen-free Hydrogen Economy. Acc. Chem. Res. 2017;50(1):74–85. https://doi.org/10.1021/acs.accounts.6b00474.
[7] Wijayanta AT, Oda T, Purnomo CW, Kashiwagi T, Aziz M. Liquid hydrogen, methylcyclohexane, and ammonia as potential hydrogen storage: Comparison review. Int J Hydrogen Energy 2019;44(29):15026–44. https://doi.org/10.1016/j.ijhydene.2019.04.112.
[8] Gianotti E, Taillades-Jacquin M, Rozière J, Jones DJ. High-Purity Hydrogen Generation via Dehydrogenation of Organic Carriers: A Review on the Catalytic Process. ACS Catal. 2018;8(5):4660–80. https://doi.org/10.1016/j.ijhydene.2019.04.112.
[9] Markiewicz M, Zhang YQ, Bösmann A, Brückner N, Thöming J, Wasserscheid P, Stolte S. Environmental and health impact assessment of Liquid Organic Hydrogen Carrier (LOHC) systems – challenges and preliminary results. Energy Environ. Sci. 2015;8(3):1035–45. https://doi.org/10.1039/c4ee03528c.
[10] Biniwale R, Rayalu S, Devotta S, Ichikawa M. Chemical hydrides: A solution to high capacity hydrogen storage and supply. Int J Hydrogen Energy 2008;33(1):360–5. https://doi.org/10.1016/j.ijhydene.2007.07.028.
[11] Usman MR. The Catalytic Dehydrogenation of Methylcyclohexane over Monometallic Catalysts for On-board Hydrogen Storage, Production, and Utilization. Energy Sources Part A 2011;33(24):2231–8. https://doi.org/10.1080/15567036.2011.565307.
[12] Akram MS, Aslam R, Alhumaidan FS, Usman MR. An exclusive kinetic model for the methylcyclohexane dehydrogenation over alumina-supported Pt catalysts. Int. J. Chem. Kinet. 2020;52(7):415–49. https://doi.org/10.1002/kin.21360.
[13] Sugiura Y, Nagatsuka T, Kubo K, Hirano Y, Nakamura A, Miyazawa K, Iizuka Y, Furuta S, Iki H, Higo T, Sekine Y. Dehydrogenation of Methylcyclohexane over Pt/TiO 2 -Al 2 O 3 Catalysts. Chem. Lett. 2017;46(11):1601–4. https://doi.org/10.1246/cl.170722.

[14] Yang X, Song Ye, Cao T, Wang L, Song H, Lin W. The double tuning effect of TiO_2 on Pt catalyzed dehydrogenation of methylcyclohexane. Molecular Catalysis 2020; 492:110971. https://doi.org/10.1016/j.mcat.2020.110971.

[15] Zhang X, He N, Lin L, Zhu Q, Wang G, Guo H. Study of the carbon cycle of a hydrogen supply system over a supported Pt catalyst: methylcyclohexane–toluene–hydrogen cycle. Catal. Sci. Technol. 2020;10(4): 1171–81. https://doi.org/10.1039/c9cy01999e.

[16] Nakaya Y, Miyazaki M, Yamazoe S, Shimizu K-I, Furukawa S. Active, selective, and durable catalyst for alkane dehydrogenation based on a well-designed trimetallic alloy. ACS Catal. 2020;10(9):5163–72. https://doi.org/10.1021/acscatal.0c00151.

[17] Hamayun MH, Maafa IM, Hussain M, Aslam R. Simulation study to investigate the effects of operational conditions on methylcyclohexane dehydrogenation for hydrogen production. Energies 2020:13. https://doi.org/10.3390/en13010206.

[18] Zhao W, Chizallet C, Sautet P, Raybaud P. Dehydrogenation mechanisms of methylcyclohexane on γ-Al_2O_3 supported Pt_{13}: Impact of cluster ductility. J Catal 2019; 370:118–29. https://doi.org/10.1016/j.jcat.2018.12.004.

[19] Chen F, Huang Y, Mi C, Wu K, Wang W, Li W, Yang Y. Density functional theory study on catalytic dehydrogenation of methylcyclohexane on Pt(111). Int J Hydrogen Energy 2020;45(11):6727–37. https://doi.org/10.1016/j.ijhydene.2019.12.096.

[20] Obodo KO, Ouma CNM, Modisha PM, Bessarabov D. Density functional theory calculation of Ti_3C_2 MXene monolayer as catalytic support for platinum towards the dehydrogenation of methylcyclohexane. Appl Surf Sci 2020;529:147186. https://doi.org/10.1016/j.apsusc.2020.147186.

[21] Bulgarin A, Jorschick H, Preuster P, Bösmann A, Wasserscheid P. Purity of hydrogen released from the Liquid Organic Hydrogen Carrier compound perhydro dibenzyltoluene by catalytic dehydrogenation. Int J Hydrogen Energy 2020;45(1): 712–20. https://doi.org/10.1016/j.ijhydene.2019.10.067.

[22] Lee S, Han G, Kim T, Yoo Y-S, Jeon S-Y, Bae J. Connected evaluation of polymer electrolyte membrane fuel cell with dehydrogenation reactor of liquid organic hydrogen carrier. Int J Hydrogen Energy 2020;45(24):13398–405. https://doi.org/10.1016/j.ijhydene.2020.02.129.

[23] Bu K, Deng J, Zhang X, Kuboon S, Yan T, Li H, Shi L, Zhang D. Promotional effects of B-terminated defective edges of Ni/boron nitride catalysts for coking- and sintering-resistant dry reforming of methane. Appl Catal B 2020;267:118692. https://doi.org/10.1016/j.apcatb.2020.118692.

[24] Do G, Preuster P, Aslam R, Bösmann A, Müller K, Arlt W, Wasserscheid P. Hydrogenation of the liquid organic hydrogen carrier compound dibenzyltoluene – reaction pathway determination by 1 H NMR spectroscopy. React. Chem. Eng. 2016;1(3):313–20. https://doi.org/10.1039/c5re00080g.

[25] Hydrogenious LOHC Technologies' ReleaseUNIT - products for hydrogen release n. d. https://www.hydrogenious.net/index.php/en/products/thereleaseunit/ (accessed June 8, 2020).

[26] Jorschick H, Preuster P, Dürr S, Seidel A, Müller K, Bösmann A, Wasserscheid P. Hydrogen storage using a hot pressure swing reactor. Energy Environ. Sci. 2017;10 (7):1652–9. https://doi.org/10.1039/c7ee00476a.

[27] Brückner N, Obesser K, Bösmann A, Teichmann D, Arlt W, Dungs J, Wasserscheid P. Evaluation of Industrially Applied Heat-Transfer Fluids as Liquid Organic Hydrogen Carrier Systems. ChemSusChem 2014;7(1):229–35. https://doi.org/10.1039/c7ee00476a.

[28] Auer F, Blaumeiser D, Bauer T, Bösmann A, Szesni N, Libuda J, Wasserscheid P. Boosting the activity of hydrogen release from liquid organic hydrogen carrier systems by sulfur-additives to Pt on alumina catalysts. Catal. Sci. Technol. 2019;9 (13):3537–47. https://doi.org/10.1039/c9cy00817a.

[29] Modisha P, Bessarabov D. Stress tolerance assessment of dibenzyltoluene-based liquid organic hydrogen carriers. Sustainable Energy Fuels 2020;4(9):4662–70. https://doi.org/10.1039/D0SE00625D.

[30] Performance of 10,000 hours of operation in Chiyoda's demo plant/ CHIYODA CORPORATION n.d. https://www.chiyodacorp.com/en/service/spera-hydrogen/demo-plant/ (accessed June 8, 2020).

[31] Okada Y, Sasaki E, Watanabe E, Hyodo S, Nishijima H. Development of dehydrogenation catalyst for hydrogen generation in organic chemical hydride method. Int J Hydrogen Energy 2006;31(10):1348–56. https://doi.org/10.1016/j.ijhydene.2005.11.014.

[32] Zaitsau DH, Emel'yanenko VN, Pimerzin AA, Verevkin SP. Benchmark properties of biphenyl as a liquid organic hydrogen carrier: Evaluation of thermochemical data with complementary experimental and computational methods. J Chem Thermodyn 2018;122:1–12. https://doi.org/10.1016/j.jct.2018.02.025.

[33] Kalenchuk AN, Bogdan VI, Dunaev SF, Kustov LM. Effect of surface hydrophilization on Pt/Sibunit catalytic activity in bicyclohexyl dehydrogenation in hydrogen storage application. Int J Hydrogen Energy 2018;43(12):6191–6. https://doi.org/10.1016/j.ijhydene.2018.01.121.

[34] Kalenchuk AN, Bogdan VI, Dunaev SF, Kustov LM. Dehydrogenation of polycyclic naphthenes on a Pt/C catalyst for hydrogen storage in liquid organic hydrogen carriers. Fuel Process Technol 2018;169:94–100. https://doi.org/10.1016/j.fuproc.2017.09.023.

[35] Kalenchuk A, Bogdan V, Dunaev S, Kustov L. Influence of steric factors on reversible reactions of hydrogenation-dehydrogenation of polycyclic aromatic hydrocarbons on a Pt/C catalyst in hydrogen storage systems. Fuel 2020;280: 118625. https://doi.org/10.1016/j.fuel.2020.118625.

[36] Gleichweit C, Amende M, Höfert O, Xu T, Späth F, Brückner N, Wasserscheid P, Libuda J, Steinrück H-P, Papp C. Surface Reactions of Dicyclohexylmethane on Pt (111). J. Phys. Chem. C 2015;119(35):20299–311. https://doi.org/10.1021/acs.jpcc.5b06178.

[37] Amende M, Kaftan A, Bachmann P, Brehmer R, Preuster P, Koch M, Wasserscheid P, Libuda J. Regeneration of LOHC dehydrogenation catalysts: In-situ IR spectroscopy on single crystals, model catalysts, and real catalysts from UHV to near ambient pressure. Appl Surf Sci 2016;360:671–83. https://doi.org/10.1016/j.apsusc.2015.11.045.

[38] Kerscher M, Klein T, Schulz PS, Veroutis E, Dürr S, Preuster P, Koller TM, Rausch MH, Economou IG, Wasserscheid P, Fröba AP. Thermophysical properties of diphenylmethane and dicyclohexylmethane as a reference liquid organic hydrogen carrier system from experiments and molecular simulations. Int J Hydrogen Energy 2020. https://doi.org/10.1016/j.ijhydene.2020.07.261.

[39] Jang M, Jo YS, Lee WJ, Shin BS, Sohn H, Jeong H, Jang SC, Kwak SK, Kang JW, Yoon CW. A High-Capacity, Reversible Liquid Organic Hydrogen Carrier: H 2 -Release Properties and an Application to a Fuel Cell. ACS Sustainable Chem. Eng. 2019;7(1):1185–94. https://doi.org/10.1021/acssuschemeng.8b04835.

[40] Han DJ, Jo YS, Shin BS, Jang M, Kang JW, Han JH, Nam SW, Yoon CW. A Novel Eutectic Mixture of Biphenyl and Diphenylmethane as a Potential Liquid Organic Hydrogen Carrier: Catalytic Hydrogenation. Energy Technol. 2019;7(1):113–21. https://doi.org/10.1002/ente.201700694.

[41] Brigljević B, Lee B, Dickson R, Kang S, Liu JJ, Lim H. Concept for Temperature-Cascade Hydrogen Release from Organic Liquid Carriers Coupled with SOFC Power Generation. Cell Reports Physical Science 2020;1(3):100032. https://doi.org/10.1016/j.xcrp.2020.100032.

[42] Lee J, Jang EJ, Kwak JH. Acid-base properties of Al_2O_3: Effects of morphology, crystalline phase, and additives. J Catal 2017;345:135–48. https://doi.org/10.1016/j.jcat.2016.11.025.

[43] Kwak JH, Hu J, Mei D, Yi CW, Kim DH, Peden CHF, et al. Coordinatively unsaturated Al^{3+} centers as binding sites for active catalyst phases of platinum on γ-Al_2O_3. Science (80-) 2009;325:1670–3. https://doi.org/10.1126/science.1176745.

[44] Sun G, Zhao Z-J, Mu R, Zha S, Li L, Chen S, Zang K, Luo J, Li Z, Purdy SC, Kropf AJ, Miller JT, Zeng L, Gong J. Breaking the scaling relationship via thermally stable Pt/Cu single atom alloys for catalytic dehydrogenation. Nat Commun 2018;9(1). https://doi.org/10.1038/s41467-018-06967-8.

[45] Al-ShaikhAli AH, Jedidi A, Anjum DH, Cavallo L, Takanabe K. Kinetics on NiZn Bimetallic Catalysts for Hydrogen Evolution via Selective Dehydrogenation of Methylcyclohexane to Toluene. ACS Catal. 2017;7(3):1592–600. https://doi.org/10.1021/acscatal.6b03299.

[46] Minemura Y, Kuriyama M, Ito S-I, Tomishige K, Kunimori K. Additive effect of alkali metal ions on preferential CO oxidation over Pt/Al_2O_3. Catal Commun 2006; 7(9):623–6.

[47] Przekop RE, Kirszensztejn P. Highly dispersed Pt on B2O3/Al2O3 support: catalytic properties in the total oxidation of 1-butene. Reac Kinet Mech Cat 2016;118(1): 325–35. https://doi.org/10.1007/s11144-016-1006-9.

[48] Xi Y, Xiao J, Lin X, Yan W, Wang C, Liu C. SiO 2 -Modified Pt/Al 2 O 3 for Oxidative Dehydrogenation of Ethane: A Preparation Method for Improved Catalytic Stability, Ethylene Selectivity, and Coking Resistance. Ind. Eng. Chem. Res. 2018; 57(31):10137–47. https://doi.org/10.1007/s11144-016-1006-9.

[49] Jo H, Jung H, Park J, Jung K-D. Surface Modification of η-Al 2 O 3 by SiO 2 Impregnation to Enhance Methanol Dehydration Activity : Surface Modification of η-Al 2 O 3. Bull. Korean Chem. Soc. 2017;38(3):307–12. https://doi.org/10.1002/bkcs.11081.

[50] Siri GJ, Bertolini GR, Casella ML, Ferretti OA. PtSn/γ-Al_2O_3 isobutane dehydrogenation catalysts: The effect of alkaline metals addition. Mater Lett 2005; 59(18):2319–24. https://doi.org/10.1016/j.matlet.2005.03.013.

[51] Zhang Y, Zhou Y, Wan L, Xue M, Duan Y, Liu X. Effect of magnesium addition on catalytic performance of PtSnK/γ-Al_2O_3 catalyst for isobutane dehydrogenation. Fuel Process Technol 2011;92(8):1632–8. https://doi.org/10.1016/j.fuproc.2011.04.011.

[52] Lieske H, Lietz G, Spindler H, Völter J. Reactions of platinum in oxygen- and hydrogen-treated Pt γ- Al_2O_3 catalysts. I. Temperature-programmed reduction, adsorption, and redispersion of platinum. J Catal 1983;81:8–16. https://doi.org/10.1016/0021-9517(83)90142-2.

[53] Contreras I, Santiago S, Pérez G, Viveros T. The Impact of a Novel Preparation Method on the Catalytic Behavior of the Pt/Al_2O_3 and Pt-Sn/Al_2O_3-Sol-Gel Catalysts for n-Heptane Reforming. Energy Fuels 2004;944:2004.

[54] Borgna A, Le Normand F, Garetto T, Apesteguia CR, Moraweck B. Sintering of Pt/Al_2O_3 reforming catalysts: EXAFS study of the behavior of metal particles under oxidizing atmosphere. Catal Lett 1992;13(3):175–88. https://doi.org/10.1007/BF00770989.

[55] Nie G, Zhang X, Pan L, Han P, Xie J, Li Z, Xie J, Zou J-J. Hydrogenated intramolecular cyclization of diphenylmethane derivatives for synthesizing high-density biofuel. Chem Eng Sci 2017;173:91–7. https://doi.org/10.1016/j.ces.2017.07.034.

[56] Radivojević D, Seshan K, Lefferts L. Preparation of well-dispersed Pt/SiO_2 catalysts using low-temperature treatments. Appl Catal A 2006;301(1):51–8. https://doi.org/10.1016/j.apcata.2005.11.016.

[57] Jaroszewska K, Masalska A, Marek D, Grzechowiak JR, Zemska A. Effect of support composition on the activity of Pt and PtMo catalysts in the conversion of n-hexadecane. Catal Today 2014;223:76–86. https://doi.org/10.1016/j.apcata.2005.11.016.

[58] Ivanova AS, Slavinskaya EM, Gulyaev RV, Zaikovskii VI, Stonkus OA, Danilova IG, Plyasova LM, Polukhina IA, Boronin AI. Metal–support interactions in Pt/Al_2O_3 and Pd/Al_2O_3 catalysts for CO oxidation. Appl Catal B 2010;97(1-2):57–71. https://doi.org/10.1016/j.apcatb.2010.03.024.